Detection and Localization of Incipient High Resistance Connection for Asymmetrical Twelve-Phase Induction Motor Drives

Detection and Localization of Incipient High Resistance Connection for Asymmetrical Twelve–Phase Induction Motor Drives

Yasser Gritli, Claudio Rossi, Gabriele Rizzoli, Luca Zarri, Angelo Tani, Domenico Casadei

***Abstract* -- Multiphase induction motors are receiving more and more interest in applications where safety and high reliability of operation are key items. Thus, condition monitoring of stator faults is crucial for guaranteeing high motor performance and efficiency. In this paper the behavior of an asymmetrical twelve-phase induction motor, with quadruple three-phase winding configuration, is investigated under high resistance connections affecting the stator windings. The analysis leads to a simple and effective methodology for detecting and localizing stator high resistance connections at incipient stage. The proposed approach is based on the computation of the voltage space vectors evaluated in the available four α–β planes. The performance of the proposed strategy is confirmed by means of numerical simulations.**

***Index Terms*— High-resistance connections, fault detection, fault localization, stator faults, multiphase induction motors, multiphase drives.**

I. INTRODUCTION

MULTIPHASE drives are nowadays well recognized as an attractive option for high current/high power applications as they provide higher efficiency and higher reliability than their three-phase counterparts [1], [2]. Their main advantages include: 1) amplitude reduction and frequency increase of torque pulsations, 2) lowering the rotor harmonic current losses and decreasing the dc link current harmonics, 3) higher fault-tolerance capabilities owing to its intrinsic active redundant structure. Thus, they are particularly adapted for energy production and transportation electrification where safety-critical is a key item, such as wind power generation systems [3], electrical ship propulsion [4], or electrical vehicles [5].

Among different topologies, multiphase induction motors based on multiple three-phase winding sets (symmetrical or asymmetrical configuration) are becoming the preferred options. Aside the reliability of the associated standard three-phase converters, multiple three-phase configuration provides an advantageous power flow modularity control, which is particularly useful in case of stator fault conditions.

In this paper, an asymmetrical twelve-phase induction motor, using a quadruple three-phase winding configuration, is investigated. As illustrated by Fig. 1, the four three-phase stator windings, with isolated neutral points, are arranged in the stator slots with a spatial shift of 15° electrical degrees. They are supplied by four independent two-level three-phase voltage source inverters. Due to the magnetic coupling among the four three-phase windings, the description of the quadruple three-phase machine is not trivial. Thus, a suitable machine model, based on multiple Space Vector Representation (SVR), has been developed [6].

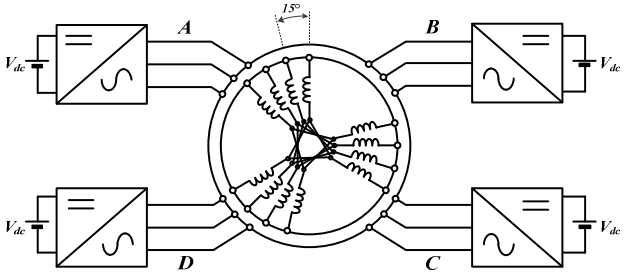

Fig. 1. Schematic diagram of the asymmetrical twelve-phase induction motor drive consisting in four voltage source inverters supplying a quadruple three-phase windings.

Although the advantages of multiphase induction motor drives in terms of fault tolerance, they are exposed to stator faults which if undetected and localized at incipient stage can lead to major damages. Thus, condition monitoring of stator faults is crucial to define the appropriate fault-tolerant strategy that can be applied by exploiting the available degrees of freedom [7]–[10]. Stator winding faults are commonly classified as short-circuit and open-circuit [11]. Other stator winding degradations are not destructive at incipient stage but can evolve and initiate serious damages to the motors. In addition to the well-known percentage (21%) of stator windings faults, established in [12], an important survey on converter reliability has revealed that 31-37.9 % of all converters failures are caused by power parts [13], [14]. Nowadays, high resistance connection (HRC) is clearly identified as a potential initiator of the stator failures. More specifically, HRC is a gradual degradation that commonly affects the motor power connections and/or the associated converters. HRC is generally caused by poor workmanship, excessive vibration levels, metal fatigue, and accentuated by overheating.

Different techniques for stator faults diagnosis and fault tolerance have been already presented in literature for three-phase induction motors [15], [16]. The classical techniques

Y. Gritli, C. Rossi, G. Rizzoli, L. Zarri, A. Tani, and D. Casadei are with the Department of Electrical, Electronic and Information Engineering "G. Marconi", University of Bologna, 40136 Bologna, Italy (emails: yasser.gritli@unibo.it, claudio.rossi@unibo.it, gabriele.rizzoli@unibo.it, luca.zarri2@unibo.it, angelo.tani@unibo.it, domenico.casadei@unibo.it). Y. Gritli is also with the Department of Electrical Engineering, University of Tunis El Manar, LA.R.A., National Engineering School of Tunis BP 37, 1002 Tunis Belvedére, Tunisia. (e-mail: yasser.gritli@ensi-uma.tn).

978-1-7281-9296-3/21/$31.00 ©2021 IEEE

for detecting high resistance connections comprise practices such as offline resistive unbalance test, infrared thermography, the voltage drop survey, and visual inspections. Recently, sensorless on-line techniques based on the zero-sequence voltage, negative sequence current, and negative-sequence regulators have been proposed for three phase induction machines [17]–[21].

For multiphase induction motors, the main contributions have been mainly oriented to the development of fault tolerant strategies more than fault diagnosis approaches [7].

In [22], a control scheme that can detect the stator resistance asymmetry in a seven-phase induction motor has been presented. More recently, an improved field-oriented control scheme for twelve-phase induction motor has been proposed in [6], where the stator asymmetry can be detected and compensated ensuring an undisturbed behavior of the induction motor drive.

Among different diagnosis strategies, signal-based methods are actually the preferred approaches [8]. In the present paper, a new simple and effective diagnosis approach is proposed for providing fast detection and localization of incipient stator high resistance connections in an asymmetrical twelve–phase induction motor drive.

II. Twelve-Phase Induction Motor Modeling

The considered machine is a 15° asymmetrical twelve-phase induction motor composed by four three-phase windings whose neutral points are isolated, as illustrated by Fig. 2.

Every three-phase winding set, namely *A*, *B*, *C*, and *D*, can be described in terms of a three-phase zero-sequence component, and a three-phase space vector. The corresponding direct and inverse transformations are given by (1)-(2) and (3)-(5), respectively.

$$x_{H0} = \frac{2}{3}\left[x_{H1} + x_{H2} + x_{H3}\right], \tag{1}$$

$$\bar{x}_H = \frac{2}{3}\left[x_{H1} + x_{H2}\,\bar{\alpha}^8 + x_{H3}\,\bar{\alpha}^{16}\right], \tag{2}$$

where $\bar{\alpha} = exp(j\pi/12)$.

$$x_{H1} = \frac{1}{2}\left[x_{H0} + \bar{x}_H + \bar{x}_H^*\right], \tag{3}$$

$$x_{H2} = \frac{1}{2}\left[x_{H0} + \bar{x}_H\,\bar{\alpha}^2 + \bar{x}_H^*\,\bar{\alpha}\right], \tag{4}$$

$$x_{H3} = \frac{1}{2}\left[x_{H0} + \bar{x}_H\,\bar{\alpha} + \bar{x}_H^*\,\bar{\alpha}^2\right]. \tag{5}$$

where the symbol "*" identifies the complex conjugate, and H = A, B, C, and D.

A. Multiple SVR

Multiple SVR is very useful for multiphase machines analysis. Here, a model for an asymmetrical twelve-phase induction motor, having four separate neutral points, has been developed by introducing six specific space vectors, which can be formulated as:

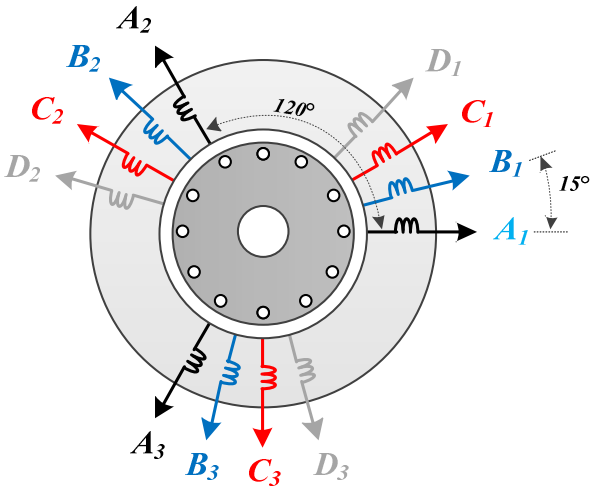

Fig. 2. Quadruple three-phase winding configuration for asymmetrical 12-phase IM.

$$\bar{y}_1 = \frac{1}{4}\left[\bar{x}_A + \bar{x}_B\,\bar{\alpha} + \bar{x}_C\,\bar{\alpha}^2 + \bar{x}_D\,\bar{\alpha}^3\right], \tag{6}$$

$$\bar{y}_5 = \frac{1}{4}\left[\bar{x}_A^* + \bar{x}_B^*\,\bar{\alpha}^5 + \bar{x}_C^*\,\bar{\alpha}^{10} + \bar{x}_D^*\,\bar{\alpha}^{15}\right], \tag{7}$$

$$\bar{y}_7 = \frac{1}{4}\left[\bar{x}_A + \bar{x}_B\,\bar{\alpha}^7 + \bar{x}_C\,\bar{\alpha}^{14} + \bar{x}_D\,\bar{\alpha}^{21}\right], \tag{8}$$

$$\bar{y}_{11} = \frac{1}{4}\left[\bar{x}_A^* + \bar{x}_B^*\,\bar{\alpha}^{11} + \bar{x}_C^*\,\bar{\alpha}^{22} + \bar{x}_D^*\,\bar{\alpha}^9\right], \tag{9}$$

Two further space vectors, depending on the four zero-sequence components, are defined as follows:

$$\bar{y}_3 = \frac{1}{4}\left[x_{A0} + x_{B0}\,\bar{\alpha}^3 + x_{C0}\,\bar{\alpha}^6 + x_{D0}\,\bar{\alpha}^9\right], \tag{10}$$

$$\bar{y}_9 = \frac{1}{4}\left[x_{A0} + x_{B0}\,\bar{\alpha}^9 + x_{C0}\,\bar{\alpha}^{18} + x_{D0}\,\bar{\alpha}^3\right]. \tag{11}$$

The corresponding inverse transformations are given by

$$\bar{x}_A = \bar{y}_1 + \bar{y}_5^* + \bar{y}_7 + \bar{y}_{11}^*, \tag{12}$$

$$\bar{x}_B = \bar{y}_1\,\bar{\alpha}^{23} + \bar{y}_5^*\,\bar{\alpha}^5 + \bar{y}_7\,\bar{\alpha}^{17} + \bar{y}_{11}^*\,\bar{\alpha}^{11}, \tag{13}$$

$$\bar{x}_C = \bar{y}_1\,\bar{\alpha}^{22} + \bar{y}_5^*\,\bar{\alpha}^{10} + \bar{y}_7\,\bar{\alpha}^{10} + \bar{y}_{11}^*\,\bar{\alpha}^{22}, \tag{14}$$

$$\bar{x}_D = \bar{y}_1\,\bar{\alpha}^{21} + \bar{y}_5^*\,\bar{\alpha}^{15} + \bar{y}_7\,\bar{\alpha}^3 + \bar{y}_{11}^*\,\bar{\alpha}^9, \tag{15}$$

and

$$x_{A0} = \bar{y}_3 + \bar{y}_3^* + \bar{y}_9 + \bar{y}_9^*, \tag{16}$$

$$x_{B0} = \bar{y}_3\,\bar{\alpha}^{21} + \bar{y}_3^*\,\bar{\alpha}^3 + \bar{y}_9\,\bar{\alpha}^{15} + \bar{y}_9^*\,\bar{\alpha}^9, \tag{17}$$

$$x_{C0} = \bar{y}_3\,\bar{\alpha}^{18} + \bar{y}_3^*\,\bar{\alpha}^6 + \bar{y}_9\,\bar{\alpha}^6 + \bar{y}_9^*\,\bar{\alpha}^{18}, \tag{18}$$

$$x_{D0} = \bar{y}_3\,\bar{\alpha}^{15} + \bar{y}_3^*\,\bar{\alpha}^9 + \bar{y}_9\,\bar{\alpha}^{21} + \bar{y}_9^*\,\bar{\alpha}^3. \tag{19}$$

B. Twelve-phase Machine Model under Healthy Condition

The analytical model of the twelve-phase induction machine, expressed in terms of multiple SVR in a stationary reference frame, can be expressed by (20)-(25) as in [6]:

$$\bar{v}_{S\rho} = R_S\,\bar{i}_{S\rho} + \frac{d\bar{\varphi}_{S\rho}}{dt} \quad ;\rho=1,5,7,11. \tag{20}$$

$$\bar{\varphi}_{S1} = L_{S1}\,\bar{i}_{S1} + M_1\,\bar{i}_{R1} \tag{21}$$

$$\bar{\varphi}_{S\rho} = L_{S\ell\rho}\,\bar{i}_{S\rho} \quad ;\rho=5,7,11. \tag{22}$$

$$0 = R_R\,\bar{i}_{R1} - j\omega\bar{\varphi}_{R1} + \frac{d\bar{\varphi}_{R1}}{dt} \tag{23}$$

$$\bar{\varphi}_{R1} = M_1\,\bar{i}_{S1} + L_{R1}\,\bar{i}_{R1} \tag{24}$$

$$T = 6pM_1\,\bar{i}_{S1}\cdot j\bar{i}_{R1} \tag{25}$$

where the stator voltage vectors and the associated stator flux vector, expressed in the ρ^{th} α-β planes, are given by (20) and (21)-(22), respectively. The rotor current vector and the rotor flux vector, expressed in the α_1-β_1 plane, are denoted as $\bar{i}_{R1}$, $\bar{\varphi}_{R1}$ respectively. The parameters L_{S1}, L_{R1}, and M_1 are the self and mutual inductances of the first α-β plane, whereas $L_{S\ell\rho}$ are the stator leakage inductances expressed in the ρ^{th} α-β planes, and p the number of pairs of poles. Finally, the electromagnetic torque is expressed by (25), where "·" denotes the scalar product. As can be seen, the variables involved in the electromagnetic torque developed by the machine are related to the α_1-β_1 plane, thus the torque control is achieved by acting on the space vector $\bar{v}_{S1}$.

Considering (20)-(22), three other decoupled sets of equations, expressed in the α_5-β_5, α_7-β_7, and α_{11}-β_{11} planes (auxiliary variables), respectively, can be identified. Since the space vectors $\bar{v}_{S5}$, $\bar{v}_{S7}$, and $\bar{v}_{S11}$ define the auxiliary stator current vectors, they must be kept contemporarily under control.

C. Twelve-phase Machine Model under HRC Condition

For a twelve-phase induction motor affected by HRC, leading to a stator resistance unbalance, the elaboration of a new analytical model is necessary. As can be seen from the previous formulation of the healthy machine established by (20)-(25), in case of stator asymmetry only the stator voltage equations (20) written in the four ρ^{th} α-β planes must be accordingly reformulated. Thus, starting from the fact that the twelve stator resistance phases can be different, the formulation of the twelve stator voltage equations is needed, which can be expressed by:

$$\begin{aligned}\bar{v}_{S1} = {} & R_{S,0}\,\bar{i}_{S1} + \bar{R}_{S,2}\,\bar{i}^*_{S1} + \bar{R}^*_{S,4}\,\bar{i}_{S5} + \bar{R}_{S,6}\,\bar{i}^*_{S5} + \\ & + \bar{R}^*_{S,6}\,\bar{i}_{S7} + \bar{R}_{S,8}\,\bar{i}^*_{S7} + \bar{R}^*_{S,10}\,\bar{i}_{S11} + R_{S,12}\,\bar{i}^*_{S11} + \frac{d\bar{\varphi}_{S1}}{dt},\end{aligned} \tag{26}$$

$$\begin{aligned}\bar{v}_{S5} = {} & \bar{R}_{S,4}\,\bar{i}_{S1} + \bar{R}_{S,6}\,\bar{i}^*_{S1} + R_{S,0}\,\bar{i}_{S5} + \bar{R}_{S,10}\,\bar{i}^*_{S5} + \\ & + \bar{R}^*_{S,2}\,\bar{i}_{S7} + R_{S,12}\,\bar{i}^*_{S7} + \bar{R}^*_{S,6}\,\bar{i}_{S11} + \bar{R}^*_{S,8}\,\bar{i}^*_{S11} + \frac{d\bar{\varphi}_{S5}}{dt},\end{aligned} \tag{27}$$

$$\begin{aligned}\bar{v}_{S7} = {} & \bar{R}_{S,6}\,\bar{i}_{S1} + \bar{R}_{S,8}\,\bar{i}^*_{S1} + \bar{R}_{S,2}\,\bar{i}_{S5} + R_{S,12}\,\bar{i}^*_{S5} + \\ & + R_{S,0}\,\bar{i}_{S7} + \bar{R}^*_{S,10}\,\bar{i}^*_{S7} + \bar{R}^*_{S,4}\,\bar{i}_{S11} + \bar{R}^*_{S,6}\,\bar{i}^*_{S11} + \frac{d\bar{\varphi}_{S7}}{dt},\end{aligned} \tag{28}$$

$$\begin{aligned}\bar{v}_{S11} = {} & \bar{R}_{S,10}\,\bar{i}_{S1} + R_{S,12}\,\bar{i}^*_{S1} + \bar{R}_{S,6}\,\bar{i}_{S5} + \bar{R}^*_{S,8}\,\bar{i}^*_{S5} + \\ & + \bar{R}_{S,4}\,\bar{i}_{S7} + \bar{R}_{S,6}\,\bar{i}^*_{S7} + R_{S,0}\,\bar{i}_{S11} + \bar{R}^*_{S,2}\,\bar{i}^*_{S11} + \frac{d\bar{\varphi}_{S11}}{dt},\end{aligned} \tag{29}$$

where

$$R_{S,0} = \frac{1}{4}\left[R_{SA0} + R_{SB0} + R_{SC0} + R_{SD0}\right], \tag{30}$$

$$\bar{R}_{S,2} = \frac{1}{4}\left[\bar{R}^*_{SA} + \bar{R}^*_{SB}\,\bar{\alpha}^2 + \bar{R}^*_{SC}\,\bar{\alpha}^4 + \bar{R}^*_{SD}\,\bar{\alpha}^6\right], \tag{31}$$

$$\bar{R}_{S,4} = \frac{1}{4}\left[\bar{R}_{SA} + \bar{R}_{SB}\,\bar{\alpha}^4 + \bar{R}_{SC}\,\bar{\alpha}^8 + \bar{R}_{SD}\,\bar{\alpha}^{12}\right], \tag{32}$$

$$\bar{R}_{S,6} = \frac{1}{4}\left[R_{SA0} + R_{SB0}\,\bar{\alpha}^6 + R_{SC0}\,\bar{\alpha}^{12} + R_{SD0}\,\bar{\alpha}^{18}\right], \tag{33}$$

where the three-phase zero-sequence resistance components R_{SA0}, R_{SB0}, R_{SC0}, R_{SD0}, and the three-phase resistance space vectors $\bar{R}_{SA}$, $\bar{R}_{SB}$, $\bar{R}_{SC}$, $\bar{R}_{SD}$ are formulated by (34) and (35), respectively.

$$R_{SH0} = \frac{1}{3}\left[R_{SH1} + R_{SH2} + R_{SH3}\right], \quad H=A,B,C,D, \tag{34}$$

$$\bar{R}_{SH} = \frac{1}{3}\left[R_{SH1} + R_{SH2}\,\bar{\alpha}^8 + R_{SH3}\,\bar{\alpha}^{16}\right], \quad H=A,B,C,D. \tag{35}$$

Owing to the star connection of each three-phase set of windings, the corresponding current zero-sequence components are equal to zero. By introducing the three-phase space vector representation, the three-phase stator voltages can be formulated as

$$\bar{v}_{SA} = \bar{v}_{S1} + \bar{v}^*_{S5} + \bar{v}_{S7} + \bar{v}^*_{S11}, \tag{36}$$

$$\bar{v}_{SB} = \bar{v}_{S1}\,\bar{\alpha}^{23} + \bar{v}^*_{S5}\,\bar{\alpha}^5 + \bar{v}_{S7}\,\bar{\alpha}^{17} + \bar{v}^*_{S11}\,\bar{\alpha}^{11}, \tag{37}$$

$$\bar{v}_{SC} = \bar{v}_{S1}\,\bar{\alpha}^{22} + \bar{v}^*_{S5}\,\bar{\alpha}^{10} + \bar{v}_{S7}\,\bar{\alpha}^{10} + \bar{v}^*_{S11}\,\bar{\alpha}^{22}, \tag{38}$$

$$\bar{v}_{SD} = \bar{v}_{S1}\,\bar{\alpha}^{21} + \bar{v}^*_{S5}\,\bar{\alpha}^{15} + \bar{v}_{S7}\,\bar{\alpha}^{3} + \bar{v}^*_{S11}\,\bar{\alpha}^{9}, \tag{39}$$

An effective stator HRC detection and localization approach, based on the developed model and more specifically on equations (30)-(33), has been developed in [6]. According to equations (26)-(29), the stator voltage space vectors, expressed in the α_1-β_1, α_5-β_5, α_7-β_7, and α_{11}-β_{11} planes, are directly affected by the HRC fault.

More specifically, under steady state operating conditions, each stator voltage space vector comprises not only a direct but also an inverse component. Thus, a simple and effective new diagnosis technique for HRC detection and localization can be based on the direct analysis of the four stator voltage space vectors $\bar{v}_{S1}$, $\bar{v}_{S5}$, $\bar{v}_{S7}$, and $\bar{v}_{S11}$, expressed by (26)-(29). According to (36)-(39), also the three-phase voltage vectors $\bar{v}_{SA}$, $\bar{v}_{SB}$, $\bar{v}_{SC}$, and $\bar{v}_{SD}$ are subsequently affected by the stator asymmetry, leading to a second alternative of signal analysis for possible detection and localization of the fault. These approaches will be fully investigated in the next sections.

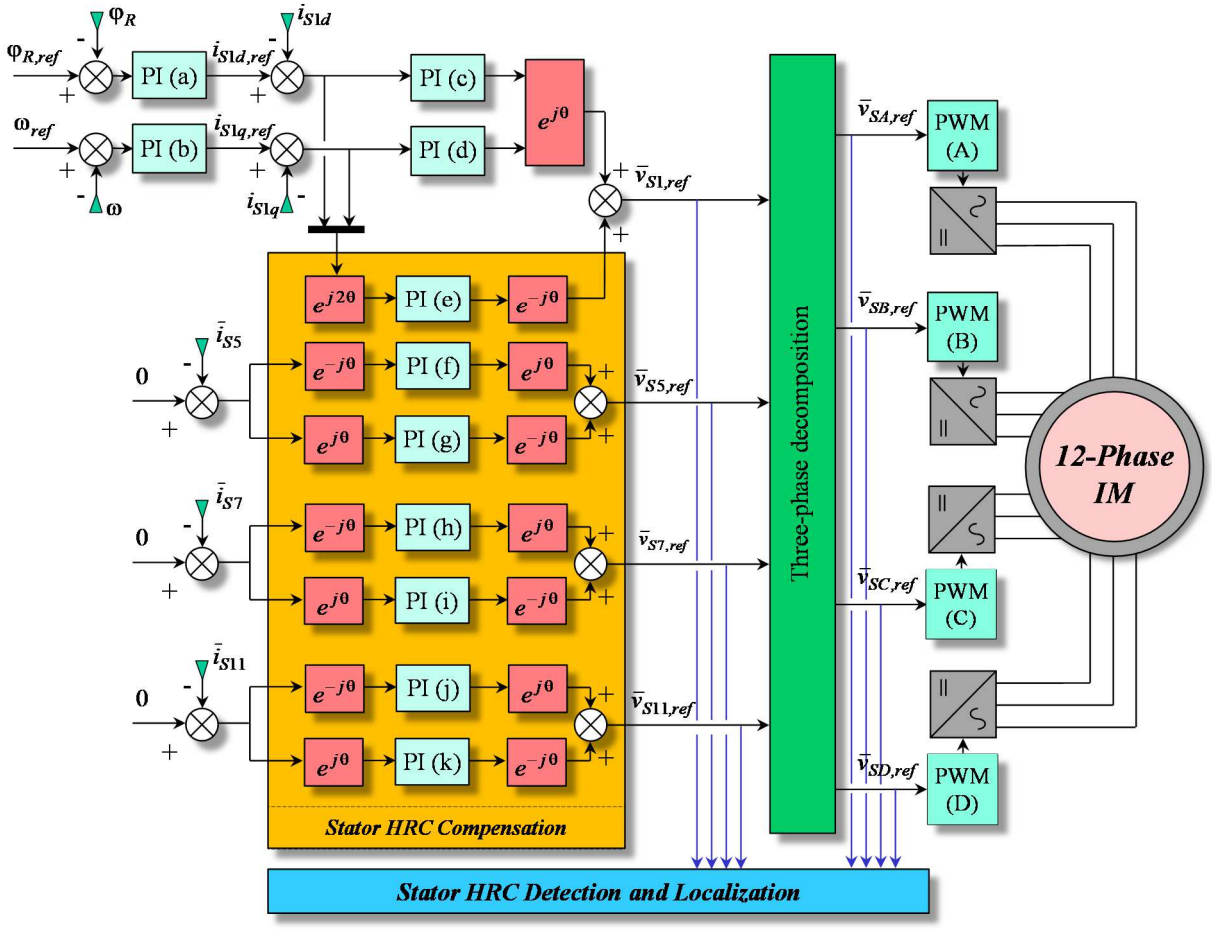

Fig. 3. Control scheme of the twelve-phase induction motor with the capability of stator asymmetry compensation.

TABLE I
TWELVE-PHASE INDUCTION MACHINE PARAMETERS

P_{rated}	= 100 kW	R_S	= 5.7 mΩ	L_{Sl5}	= 43.4 μH
$I_{S,\,rated}$	= 113 A_{rms}	R_R	= 6.1 mΩ	L_{Sl7}	= 41.7 μH
$V_{S,rated}$	= 150 V_{rms}	L_{S1}	= 2.67 mH	L_{Sl11}	= 77.7 μH
$f_{S,rated}$	= 200 Hz	L_{R1}	= 2.71 mH		
p	= 2 (pairs)	M_1	= 2.59 mH		

III. STATOR DISTURBANCE-FREE CONTROL SCHEME

The twelve-phase induction motor control scheme is based on a rotor Field-Oriented Control (FOC) scheme, ensuring a decoupled regulation of torque, and rotor flux (Fig. 3). The current regulators PI(c) and PI(d), which are implemented in a reference frame synchronized with the rotor flux, are adopted to track the current references.

The basic control configuration has been enhanced in such a way that the machine operation is not affected by stator asymmetries. More specifically, under healthy condition, the current space vectors $\bar{i}_{S5}$, $\bar{i}_{S7}$, and $\bar{i}_{S11}$ are theoretically equal to zero. However, when the stator symmetry is lost, the proposed control system is designed to apply the appropriate voltages, so these currents are maintained equal to zero. Therefore, a stator disturbance-free operation of the multiphase drive is ensured. Hence, to compensate the negative effects of these fault components, pairs of PI regulators (PI(e), PI(f), PI(g), ..., PI(j), PI(k)) implemented in two reference frames rotating in the same and in the opposite direction of the field-oriented reference frame, have been implemented in each plane. Finally, it is important to notice that the regulator gains tuning is not critical, and it has been made by trial-and-error method.

IV. SIMULATION RESULTS

To investigate the performance of the proposed approach for stator fault detection and localization, the twelve-phase induction motor controlled by the proposed control scheme have been implemented in Matlab/Simulink. The machine parameters are reported in Table I. The DC bus voltage for each three-phase VSI is of 215 V, where the switching period is of 100 μs. All simulations have been carried out running the induction motor at constant speed of 3000 rpm, and the rotor flux and torque references are maintained constant at rated values (0.092 Wb, 160 Nm).

Initially, the behavior of the induction machine has been tested under healthy condition, where the twelve stator phase resistances are identical and equal to R_s. Then, for the same rated operating point, an additional resistance, equal to 50% of the rated resistance R_s, is added to phase A1. The four figures (Fig. 4 to Fig. 7) show the behavior of the drive, in terms of loci of the voltage space vectors expressed in the

four α-β planes, respectively, under healthy and faulty operating conditions. As can be seen in Fig. 4, the locus of the voltage space vector $\bar{v}_{S1}$ is circular for healthy condition (Fig. 4-a), as well as under faulty operating conditions (Fig. 4-b). This result ensures a good performance of the twelve-hase machine in terms of torque ripple. The corresponding loci of the voltage space vector $\bar{v}_{S5}$, are reported in Fig. 5-a and Fig. 5-b, respectively, where the behavior of the drive is very different from healthy to faulty conditions. More specifically, under healthy condition, the locus of $\bar{v}_{S5}$ is zero (Fig. 5), which is expected by the control system, where the set point of $\bar{i}_{S5}$ is assumed equal to zero (Fig. 3). However, under faulty condition, the voltage space vector $\bar{v}_{S5}$ increase sensibly as shown in Fig. 5-b, which justify the existence of a direct and inverse components as expected by equation (27). Observing the corresponding loci of the voltage space vectors $\bar{v}_{S7}$ and $\bar{v}_{S11}$, depicted in Fig. 6 and Fig. 7, respectively, the same observations can be made. In fact, the reported results shown in Fig. 6-b and Fig. 7-b were analytically predicted by equations (28) and (29), where the contributions of a direct and an inverse component due to the presence of HRC is expected. At this point of the investigations, the loci of the voltage space vectors $\bar{v}_{S5}$, $\bar{v}_{S7}$ and $\bar{v}_{S11}$ have shown significant shape variations, from healthy to faulty condition, leading to an interesting stator HRC fault signature for this type of multiphase induction machines. The established detection approach, which allows a clear discrimination between healthy and stator fault operating condition, can be quantitatively emphasized by spectral analysis of the respective ρ^{th} voltage space vectors. The spectra of the voltage space vectors $\bar{v}_{S1}$, $\bar{v}_{S5}$, $\bar{v}_{S7}$ and $\bar{v}_{S11}$ are depicted in Fig. 8-Fig. 11, respectively, under healthy and stator HRC. The spectra of $\bar{v}_{S1}$ under healthy, and faulty condition are reported in (Fig. 8-a) and (Fig. 8-b), respectively, where the dominance of the fundamental component can be clearly evidenced for both cases, which confirm the circular behaviors observed in Fig. 4-a, as well as in Fig. 4-b for the faulty case. It should be noted that under a 50% of stator unbalance affecting phase A1, the inverse component has shown a relevant amplitude of approximately -30 dB.

Comparing the spectra of $\bar{v}_{S5}$ under healthy (Fig. 9-a), and faulty (Fig. 9-b) condition, the contributions of the direct and inverse components, from healthy to stator fault condition, can be clearly evidenced with amplitudes of approximately -30 dB (Fig. 9-b). It is worth noting that this result is in a complete accordance with the analytical formulation of the voltage space vector $\bar{v}_{S5}$ formulated in (27), and confirm the loci behavior of Fig. 5. The same conclusions can be made when examining the spectra corresponding to the voltage space vectors $\bar{v}_{S7}$ and $\bar{v}_{S11}$, reported in Fig. 10 and Fig. 11, respectively under healthy

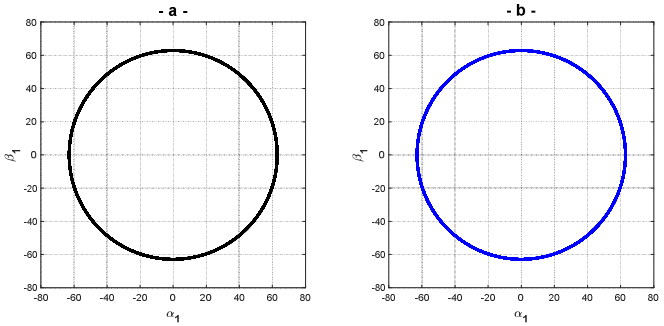

Fig. 4. Loci of the voltage space vectors, in the α_1-β_1 plane, under a) healthy condition, and b) stator asymmetry of 50% in phase-A1. The vector-controlled machine is rotating at constant speed of 3000 rpm, and under the rated torque of 160 Nm.

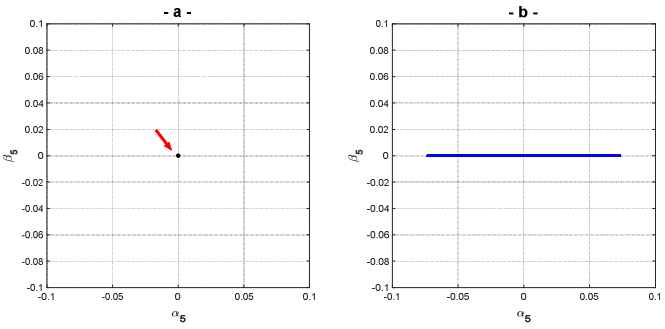

Fig. 5. Loci of the voltage space vectors, in the α_5-β_5 plane, under a) healthy condition, and b) stator asymmetry of 50% in phase-A1. The vector-controlled machine is rotating at constant speed of 3000 rpm, and under the rated torque of 160 Nm.

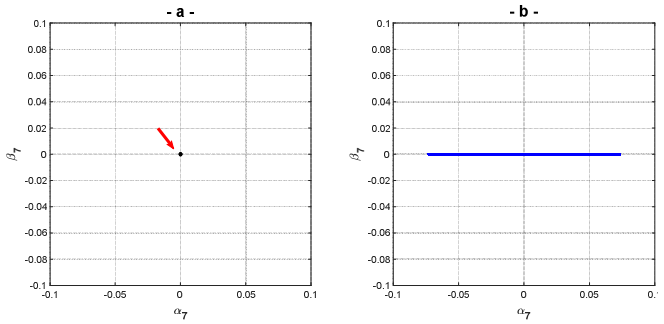

Fig. 6. Loci of the voltage space vectors, in the α_7-β_7 plane, under a) healthy condition, and b) stator asymmetry of 50% in phase-A1. The vector-controlled machine is rotating at constant speed of 3000 rpm, and under the rated torque of 160 Nm.

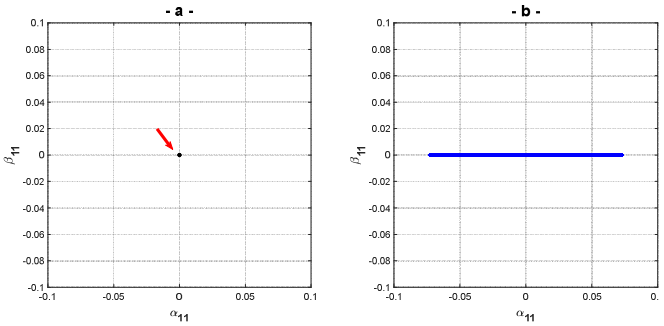

Fig. 7. Loci of the voltage space vectors, in the α_{11}-β_{11} plane, under a) healthy condition, and b) stator asymmetry of 50% in phase-A1. The vector-controlled machine is rotating at constant speed of 3000 rpm, and under the rated torque of 160 Nm.

and stator HRC. At this level of investigations, the amplitude variation of the direct and inverse components emerged under faulty condition, can be adopted as reliable fault indexes for detecting and quantifying stator HRC affecting a twelve-phase induction motor. Once the fault is detected, the localization of the fault is a key step for defining actions to be taken, and mainly the appropriate fault-tolerant strategy that can be applied by exploiting the available degrees of freedom. Loci of the voltage space vectors $\bar{v}_{S1}$, $\bar{v}_{S5}$, $\bar{v}_{S7}$ and $\bar{v}_{S11}$, under different stator asymmetries of 50% affecting phase A1, phase C3, phase D1, and phase-B2, are reported in Fig. 12a-Fig. 12d, respectively. Observing the angle variations adopted by each locus of the voltage space vectors $\bar{v}_{S5}$, $\bar{v}_{S7}$, and $\bar{v}_{S11}$, according to the fault location cases, leads to an effective identification of the phase affected by the stator HRC. As already analytically established by equations (36)-(39), the reference voltage space vectors $\bar{v}_{SA}$, $\bar{v}_{SB}$, $\bar{v}_{SC}$ and $\bar{v}_{SD}$, are also affected in case of stator HRC. In Fig. 13, the spectra of the voltage space vectors $\bar{v}_{SA}$, $\bar{v}_{SB}$, $\bar{v}_{SC}$ and $\bar{v}_{SD}$, under a stator asymmetry of 50% in phase-A1, are reported. As can be seen only the voltage space vector $\bar{v}_{SA}$ is concerned by a relevant inverse component (~ -12 dB), which allows not only the quantification of the stator HRC but also to localize the three-phase windings and/or the associated three-phase inverter affected by the fault. This approach is also confirmed by a second case of stator HRC affecting phase B2 (Fig. 14), where only the spectrum of the corresponding voltage space vector $\bar{v}_{SB}$ (Fig. 14) has shown a relevant inverse component.

The voltage spectra of $\bar{v}_{SA}$, $\bar{v}_{SB}$, $\bar{v}_{SC}$ and $\bar{v}_{SD}$ have been analyzed for all cases of single-phase machine affected by stator HRC. Only the space vector corresponding to the three-phase winding, affected by the fault, has shown a relevant inverse component, leading to an effective and simple approach for stator HRC detection and localization in twelve-phase induction motor.

V. Conclusion

In this paper, the behavior of a multiphase induction motor was investigated under the assumption that the stator winding is affected by an incipient stator high resistance connection. The analysis leads to a new simple and effective diagnosis approach for detecting and localizing stator high resistance connection in a twelve-phase induction motor.

The proposed approach is based on the exploitation of the different degrees of freedom of the twelve-phase drive, where the control system provides suitable signals that are exploited for detecting and localizing the stator fault. The theoretical analysis is confirmed by numerical simulations of the multiple space vector-based modeling of the investigated twelve-phase induction motor drive.

Finally, further analysis of the proposed approach, against the control parameters and the operating conditions, are needed. This will be the subject of a future paper.

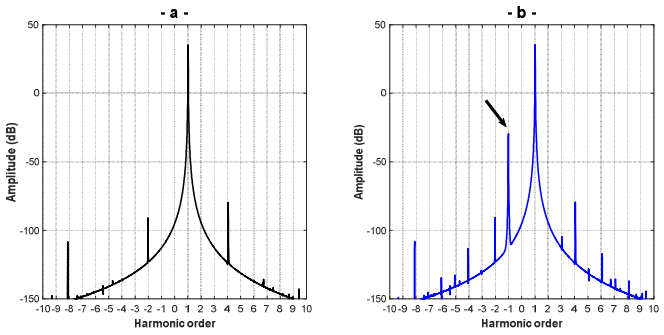

Fig. 8. Spectra of the voltage space vectors, in the α_1-β_1 plane, under a) healthy condition, and b) stator asymmetry of 50% in phase-A1. The vector-controlled machine is rotating at constant speed of 3000 rpm, and under the rated torque of 160 Nm.

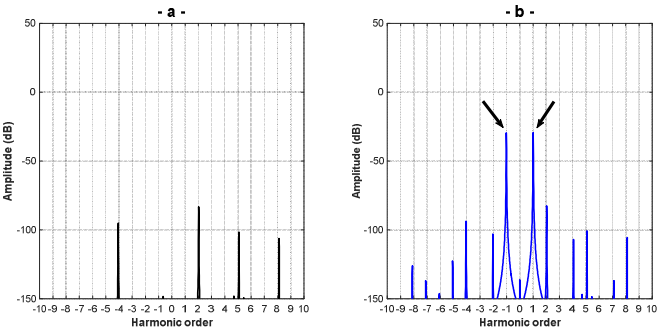

Fig. 9. Spectra of the voltage space vectors, in the α_5-β_5 plane, under a) healthy condition, and b) stator asymmetry of 50% in phase-A1. The vector-controlled machine is rotating at constant speed of 3000 rpm, and under the rated torque of 160 Nm.

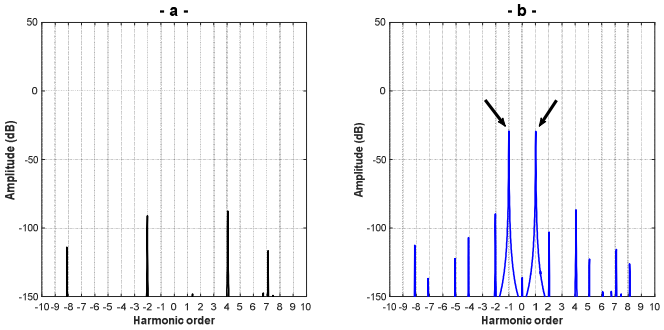

Fig. 10. Spectra of the voltage space vectors, in the α_7-β_7 plane, under a) healthy condition, and b) stator asymmetry of 50% in phase-A1. The vector-controlled machine is rotating at constant speed of 3000 rpm, and under the rated torque of 160 Nm.

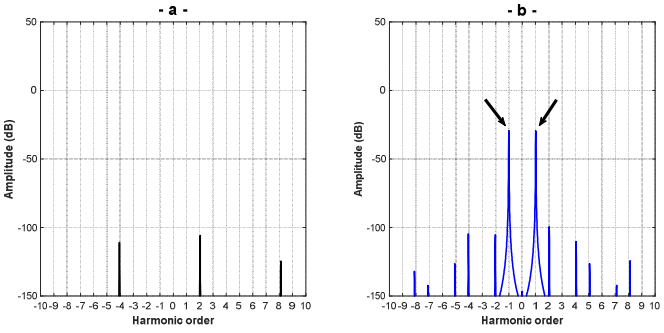

Fig. 11. Spectra of the voltage space vectors, in the α_{11}-β_{11} plane, under a) healthy condition, and b) stator asymmetry of 50% in phase-A1. The vector-controlled machine is rotating at constant speed of 3000 rpm, and under the rated torque of 160 Nm.

VI. REFERENCES

[1] E. Levi, R. Bojoi, F. Profumo, H. A. Toliyat, and S. Williamson, "Multiphase induction motor drives–a technology status review," *IET Electr. Power Appl.*, vol. 1, no. 4, pp. 489–516, 2007.

[2] E. Levi, "Multiphase electric machines for variable-speed applications," *IEEE Trans. Ind. Electron.*, vol. 55, no. 5, pp. 1893–1909, 2008.

[3] I. Gonzalez, M. Duran, F. Barrero, M. Bermudez, and H. Guzman, "Fault-tolerant Efficient Control of a Six-phase Induction Machine with Parallel Machine-side Converters," *IEEE Trans. Power Electron.*, no. 99, p. 1, 2016.

[4] F. Terrien, S. Siala, and P. Noy, "Multiphase induction motor sensorless control for electric ship propulsion," in *Proc. IEE PEMD Conf., Edinburgh, UK*, 2004, pp. 556–561.

[5] R. Bojoi, A. Cavagnino, M. Cossale, A. Tenconi, and S. Vaschetto, "Design trade-off and experimental validation of multiphase starter generators for 48v mini-hybrid powertrain," in *2014 IEEE International Electric Vehicle Conference (IEVC)*, 2014, pp. 1–7.

[6] A. Tani, L. Zarri, M. Mengoni, G. Serra, and D. Casadei, "Detection and localization of high resistance connections in quadruple three-phase induction motor drives," in *2014 International Conference on Electrical Machines (ICEM)*, 2014, pp. 2094–2100.

[7] M. J. Duran and F. Barrero, "Recent advances in the design, modeling, and control of multiphase machines - Part II," *IEEE Trans. Ind. Electron.*, vol. 63, no. 1, pp. 459–468, 2016.

[8] Z. Gao, C. Cecati, and S. X. Ding, "A survey of fault diagnosis and fault-tolerant techniques—Part I: Fault diagnosis with model-based and signal-based approaches," *IEEE Trans. Ind. Electron.*, vol. 62, no. 6, pp. 3757–3767, 2015.

[9] Z. Gao, C. Cecati, and S. X. Ding, "A survey of fault diagnosis and fault-tolerant techniques—Part II: Fault diagnosis with knowledge-based and hybrid/active approaches," *IEEE Trans. Ind. Electron.*, vol. 62, no. 6, pp. 3768–3774, 2015.

[10] E. Levi, "Advances in converter control and innovative exploitation of additional degrees of freedom for multiphase machines," *IEEE Trans. Ind. Electron.*, vol. 63, no. 1, pp. 433–448, 2016.

[11] A. Bellini, F. Filippetti, C. Tassoni, and G.-A. Capolino, "Advances in diagnostic techniques for induction machines," *IEEE Trans. Ind. Electron.*, vol. 55, no. 12, pp. 4109–4126, 2008.

[12] A. H. Bonnett and C. Yung, "Increased efficiency versus increased reliability," *IEEE Ind. Appl. Mag.*, vol. 14, no. 1, pp. 29–36, 2008.

[13] M. H. Standard, "Reliability prediction of electronic equipment," *Mil. Handb. MIL-HDBK-217E, Not.*, vol. 1, 1990.

[14] A. L. Julian and G. Oriti, "A comparison of redundant inverter topologies to improve voltage source inverter reliability," *IEEE Trans. Ind. Appl.*, vol. 43, no. 5, pp. 1371–1378, 2007.

[15] H. Henao *et al.*, "Trends in fault diagnosis for electrical machines: A review of diagnostic techniques," *IEEE Ind. Electron. Mag.*, vol. 8, no. 2, pp. 31–42, 2014.

[16] D. U. Campos-Delgado, D. R. Espinoza-Trejo, and E. Palacios, "Fault-tolerant control in variable speed drives: a survey," *IET Electr. Power Appl.*, vol. 2, no. 2, pp. 121–134, 2008.

[17] J. Yun, K. W. Lee, K. W. Lee, S. Bin Lee, and J. Y. Yoo, "Detection and classification of stator turn faults and high-resistance electrical connections for induction machines," *IEEE Trans. Ind. Appl.*, vol. 45, no. 2, pp. 666–675, 2009.

[18] J. Yun, J. Cho, S. Bin Lee, and J.-Y. Y. Yoo, "Online detection of high-resistance connections in the incoming electrical circuit for induction motors," *IEEE Trans. Ind. Appl.*, vol. 45, no. 2, pp. 694–702, 2009.

[19] Y. Gritli, L. Zarri, C. Rossi, F. Filippetti, G.-A. G. A. Capolino, and D. Casadei, "Advanced diagnosis of electrical faults in wound-rotor induction machines," *IEEE Trans. Ind. Electron.*, vol. 60, no. 9, pp. 4012–4024, 2013.

[20] M. Mengoni, L. Zarri, Y. Gritli, A. Tani, F. Filippetti, and S. Bin Lee, "Online Detection of High-Resistance Connections With Negative-Sequence Regulators in Three-Phase Induction Motor Drives," *IEEE Trans. Ind. Appl.*, vol. 51, no. 2, pp. 1579–1586, 2015.

[21] S. K. Kommuri, Y. Park, and S. Bin Lee, "High-Resistance Fault-Control in Permanent Magnet Synchronous Motors," *IEEE/ASME Trans. Mechatronics*, vol. 25, no. 1, pp. 271–281, 2020.

[22] L. Zarri *et al.*, "Detection and localization of stator resistance dissymmetry based on multiple reference frame controllers in multiphase induction motor drives," *IEEE Trans. Ind. Electron.*, vol. 60, no. 8, pp. 3506–3518, 2013.

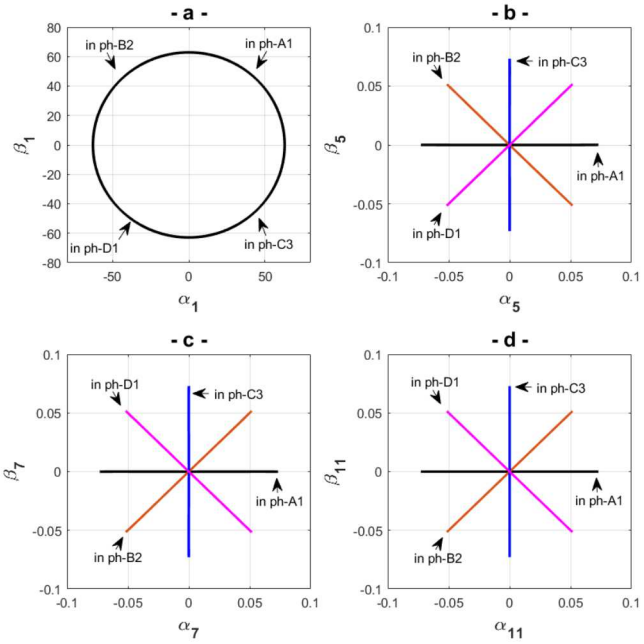

Fig. 12. Loci of the voltage space vectors, in the a) α_1-β_1 , b) α_5-β_5 , c) α_7-β_7 , and d) α_{11}-β_{11} planes, under different stator asymmetries of 50% affecting phase A1 (black trace), phase C3 (blue trace), phase D1(magenta trace), and phase-B2 (red trace). The vector-controlled machine is rotating at constant speed of 3000 rpm, and under the rated torque of 160 Nm.

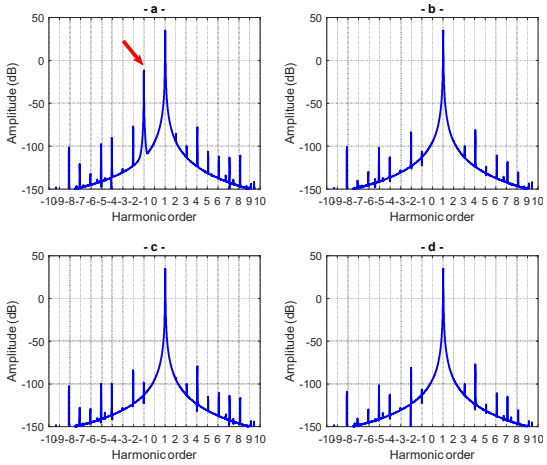

Fig. 13. Spectra of the voltage space vectors a) $\bar{v}_{SA}$, b) $\bar{v}_{SB}$, c) $\bar{v}_{SC}$ and d) $\bar{v}_{SD}$, under a stator asymmetry of 50% in phase-A1.

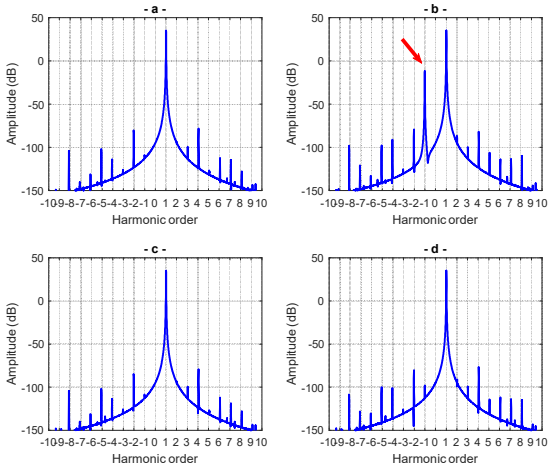

Fig. 14. Spectra of the voltage space vectors a) $\bar{v}_{SA}$, b) $\bar{v}_{SB}$, c) $\bar{v}_{SC}$ and d) $\bar{v}_{SD}$, under a stator asymmetry of 50% in phase-B2.